PCCP

PAPER

View Article Online
View Journal | View Issue

Cite this: *Phys. Chem. Chem. Phys.*, 2016, **18**, 14709

Synthesis and structure–property relationships of phthalimide and naphthalimide based organic π-conjugated small molecules†

Abby-Jo Payne,‡[a] Arthur D. Hendsbee,‡[a] Seth M. McAfee,[a] Devproshad K. Paul,[b] Kunal Karan[b] and Gregory C. Welch*[a]

Received 8th March 2016,
Accepted 7th May 2016

DOI: 10.1039/c6cp01596d

www.rsc.org/pccp

Five organic π-conjugated small molecules with bithiophene-phthalimide backbones bearing alkyl chains of different symmetry, length and branching character were synthesized using optimized microwave and direct heteroarylation protocols. The chosen alkyl chains were 1-ethylpropyl, 1-methylbutyl, pentyl, hexyl and octyl. A sixth compound was also synthesized replacing the phthalimide terminal units with octylnaphthalimide for additional scope. Through the thorough analysis of both thermal and optical properties and the investigation of self-assembly tendencies by single crystal X-ray diffraction and variable angle spectroscopic ellipsometry it is evident that alkyl side chains and building block size influence many facets of material properties. Within this class of materials the 1-ethylpropyl derivative exhibited the most unique behaviour.

Introduction

The use of organic donor–acceptor (D–A) π-conjugated materials as active components in electronic devices has been exploited for numerous applications, including: sensors, thin-film transistors and photovoltaic cells.[1–3] The key advantage of D–A compounds relates to the ability to tailor material properties such as electronic energy levels, optical absorption profiles, solubility parameters and self-assembly tendencies.[4–6] The synthetic chemist can precisely control these properties with versatile synthetic methods that are adaptable to modifications in the selection and functionalization of the donor and acceptor building blocks. While the derivatization of established π-conjugated organic materials is dominated by the investigation of new organic building blocks and electron-donating or -withdrawing substituents, varying the alkyl side chains has become increasingly important for understanding the structure–property relationships of new materials.

With the on-going development of solution-processable D–A π-conjugated materials, side chain engineering has emerged as an important avenue to explore for fine-tuning the properties of an established functional material. It is understood that the influence of solubilizing alkyl side chains is not limited to promoting material solubility, and has been shown to play a crucial role in the self-assembly tendencies, impacting opto-electronic properties and performance. For extensive details on the influences of side chain engineering in organic π-conjugated materials we direct the reader to a couple of recent reviews.[7,8]

Alkyl side chains can be broadly classified into two categories based on their structure being either linear or branched. Linear alkyl chains are often modified through alteration to the length of the side chain in view of increased material solubility;[9,10] however, a trade-off exists, and modifying the side chain beyond a certain length (often unique for any given material) can hinder material performance. The modification to side chain length is regularly made through an increase or decrease by two carbon units due to the odd–even effect. Not only are even carbon length side chains more readily accessible, but they have also demonstrated improved material performance.[11,12] This odd–even influence is often related to molecular symmetry and the vital role it plays in single crystal packing.

The use of a branched alkyl chain in place of the linear variety was initially conceived as a means to provide greater solubilizing capability through the steric disruption of side chain interdigitation, a prevalent concern with linear alkyl chains. Lacking the propensity for this aggregation behaviour, branched alkyl side chains have been shown to adopt different

[a] *Department of Chemistry, University of Calgary, 2500 University Drive N.W., Calgary, Alberta, Canada T2N 1N4. E-mail: greogry.welch@ucalgary.ca*
[b] *Department of Chemical and Petroleum Engineering, Schulich School of Engineering, University of Calgary, 2500 University Drive N.W., Calgary, Alberta, Canada T2N 1N4*

† Electronic supplementary information (ESI) available: Experimental details, ^{1}H and ^{13}C NMR spectra, additional UV-vis and PL spectra, optical microscopy images, DSC thermograms of compound 1 run at different rates, additional VSE plots, and details on OFET fabrication and testing. CCDC 1435601–1435604. For ESI and crystallographic data in CIF or other electronic format see DOI: 10.1039/c6cp01596d

‡ Authors contributed equally.

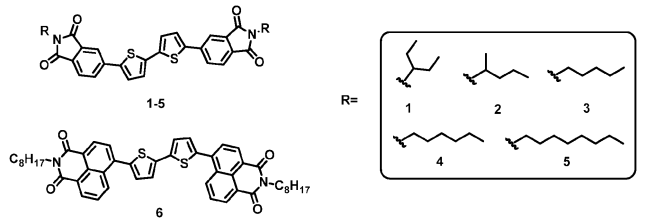

Fig. 1 Structures of compounds **1–6**. Compound **6** incorporates linear octyl chains.

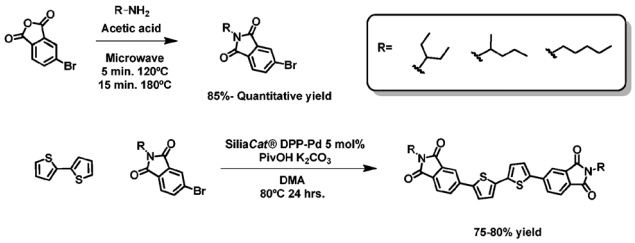

Fig. 2 Synthesis of compounds **1–3**.

solid-state orientations than their linear counterparts leading to significant influence on performance metrics.[13–15] Depending on the location of the branching site, these alkyl side chains can be either symmetrical or asymmetric, and each offer distinctive variations to molecular conformation, contributing to different molecular properties and performance.[16]

In this work we investigate the side chain engineering of a well-studied D–A π-conjugated molecular framework synthesized in our group, 5,5′(2,2′-bithiophene-5,5′-diyl)bis(2-alkylphthalimide).[17–22] In this D–A framework, the bithiophene electron-rich core (D) is flanked with electron-deficient imide terminal units (A). Imide-flanked materials have shown considerable success in organic π-conjugated materials,[23–26] and are attractive due to their well-studied self-assembly properties, and the ability to functionalize the imido-nitrogen with a wide range of alkyl side chains. The favourable hole and electron mobilities of the hexyl derivative in evaporated field-effect transistors (FETs) has already been demonstrated by our group,[19] thus warranting further fundamental investigation of these materials.

The influence of side chain engineering will be primarily focused on the phthalimide terminal acceptor,[27–29] but will be supplemented with one naphthalimide-terminated material,[30–33] to demonstrate the optoelectronic influence of altering the terminal acceptor in this case, rather than the alkyl side chain. The side chains selected for this work are primarily focused on the 5-carbon family of 1-ethylpropyl alkyl groups. 1-Ethylpropyl side chains have been widely used for solubilizing many π-conjugated materials in the literature particularly those based on perylene diimide (PDI),[22,29,34–38] but to the best of our knowledge, it has never been directly compared with other 5-carbon side chains. For this reason, we have investigated the influence of the symmetrical branched 1-ethylpropyl side chains in comparison with the asymmetric branched 1-methylbutyl and the linear pentyl. Within this family of side chains we can probe the influence of branching points and symmetry. Extending the scope to our previously reported hexyl and octyl derivatives we have also been able to supplement this investigation with the impact of the odd–even effect and the influence of increasing the length of linear side chains (Fig. 1).

Results and discussion

Synthesis

Compounds **1–3** were prepared through a simple two-step synthesis utilizing optimized microwave and direct heteroarylation reactions[21] (Fig. 2). To access the alkylated 4-bromophthalimide precursors, 4-bromophthalic anhydride was condensed with the desired alkyl amine in acetic acid for five minutes at 120 °C followed by 15 minutes at 180 °C under microwave irradiation. The cooled reaction mixture was then poured into water and the resulting white precipitate was isolated by vacuum filtration, washing with 3 : 1 water : methanol. The alkylated products were successfully synthesized and isolated as white powders in high yields (>85%). Final materials **1–3** were then synthesized by direct heteroarylation, where two equivalents of the desired alkylated 4-bromo-phthalimide were reacted with one equivalent of 2,2′-bithiophene in dimethylacetamide (DMA) with pivalic acid, potassium carbonate and SiliaCat® DPP-Pd as the supported catalyst. The cooled reaction mixtures were then poured into water. The resulting orange precipitates were collected *via* vacuum filtration, dissolved in ethyl acetate and filtered through a short silica plug to remove the catalyst and residual inorganic solids. The materials were further purified by recrystallization from tetrahydrofuran (THF) yielding compounds **1–3** as bright orange solids in appreciable yields (75–80%).

Compounds **4** and **5** were prepared as previously reported by our group.[22] Compound **6**; however, was prepared by an alternative synthetic route where the backbone precursors were first pieced together using a Stille reaction followed by alkylation as the final step (Fig. 3). The un-alkylated product was prepared through the reaction of two equivalents of 4-bromo-1,8-naphthalic anhydride and one equivalent of 5,5′-bis(trimethylstannyl)-2,2′-bithiophene in anhydrous toluene with $Pd(PPh_3)_4$ as the catalyst. The reaction mixture was heated under microwave irradiation for five minutes at 100 °C followed by 20 minutes at 170 °C. The cooled reaction mixture was poured into methanol. In order to

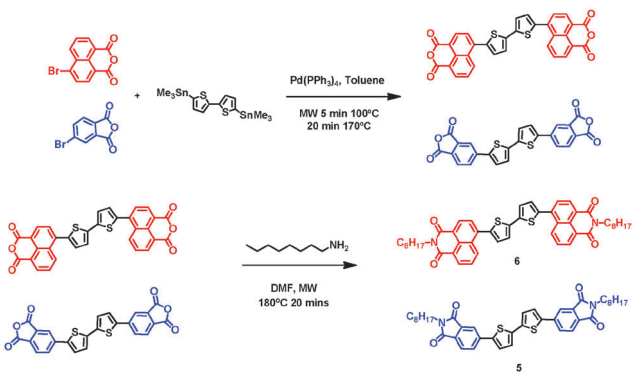

Fig. 3 Synthesis of compounds **5** and **6**.

remove trace catalyst and tin impurities the resulting brown solid was heated in isopropanol then THF and collected *via* vacuum filtration as a brown-red solid (81% yield). Due to low solubility, the product 6,6′-([2,2′-bithiophene]-5,5′-diyl)bis-(naphthalimide) (**Nap-Th$_2$-Nap**) could only be identified by mass spectrometry (APCI-TOF). **Nap-Th$_2$-Nap** was subsequently reacted with an excess of octylamine in anhydrous dimethylformamide (DMF) in a microwave reactor at 180 °C for 20 minutes. The cooled reaction mixture was poured into water and the resulting product was filtered to collect a solid, which was then solubilized in dichloromethane and sent through a short silica plug to remove any residual insoluble starting material. The solvent was removed under reduced pressure and the solid was slurried in 3 : 1 water : methanol and isolated using vacuum filtration to yield **6** as a pure orange solid with no further purification required (89% yield). The same reaction and work-up conditions were also successfully applied in synthesizing 5 with octylphthalimide end-caps as an alternative synthetic method resulting in materials requiring no recrystallization or column chromatography as previously reported.[17,19]

All synthesized compounds were identified by ^{1}H NMR spectroscopy and unreported compounds were further characterized by ^{13}C NMR spectroscopy and mass spectrometry (APCI-TOF).

Optical properties

The UV-vis absorption spectra of the final compounds were obtained from 1% wt/v solutions in chloroform. The solution profiles were obtained from diluted solutions and thin films were spun cast onto glass substrates. Both solution and thin-film absorption profiles are shown in Fig. 4 and the data summarized in Table 1. In solution, compounds **1–5** are nearly identical, as expected, having the same π-conjugated backbone with an absorption onset of 485 nm and absorption maximum at 425 nm. Changing the endcap from phthalimide to 1,8-naphthalimide, results in a slight red shift of the absorption max by <5 nm and a broadening of the profile to 505 nm. The emergence of a high-energy shoulder also appears at 335 nm. It is in the thin film absorption measurements, where it becomes obvious the side chains have varying impacts on the self-assembly properties. For all compounds a red shift in the onset is observed out to ~500 nm. Compounds **1** and **2** with the branched alkyl chains maintain their absorption maxima with an overall broadening of the absorption profile with a slight shoulder appearing at 460 nm. In contrast, compounds **3–5** with linear side chains all show a blue shift in absorption maximum to 388 nm. These blue shifts can be characteristic of H-aggregates, which aggregate in a face-to-face π-stacking fashion.[39–41] This packing motif has been shown to lead to high charge carrier mobilities in FETs.[17,19,42–45] Compound **6** with octylnaphthalimide end-caps is similar to compounds **1** and **2**, showing no shift in absorption maximum upon transitioning from solution to thin film but sees the largest red shift in absorption onset from 505 nm to 540 nm.

In addition to optical absorption, photoluminescence (PL) measurements were conducted (Fig. S13 and S14, ESI†) with the data summarized in Table 1. Phthalimide compounds **1–6** are all emissive in solution ($CHCl_3$) with similar stokes shifts ranging from 76–89 nm, which is not surprising considering the identical backbone structure. Compound **6** exhibits a larger stoke shift of 117 nm, which is likely attributed to the increased torsional strain of the backbone as a result of the bulkier 1,8-naphthalimide endcaps. The emission profiles for the thin films (Fig. S14, ESI†) displayed more variation in stokes-shifts between the compounds but were overall slightly red-shifted from solution.

To investigate the influence of side chains on the structure–property relationships in this class of molecules the effect of thermal annealing on the thin films were explored using UV-vis spectrometry and optical microscopy (Fig. S11, ESI†).

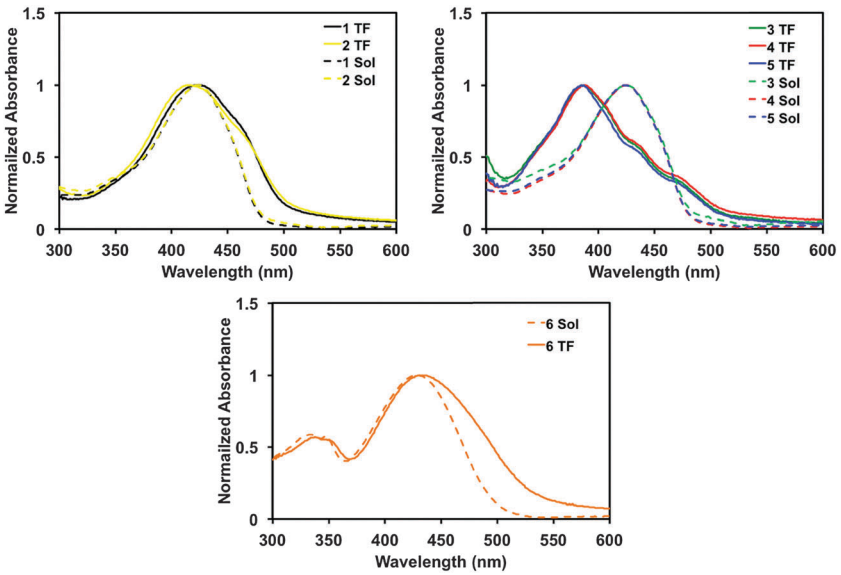

Fig. 4 UV-vis absorption of small molecules **1–6** in $CHCl_3$ (Sol) or as thin-films (TF) cast from $CHCl_3$. Absorption profiles in solution (dashed lines) and as-cast spin coated films (dark solid lines).

Table 1 Optical and thermal properties of compounds **1–6**

	1	2	3	4	5	6
UV-vis absorbance						
Solution λ_{onset} (nm)	485	485	485	485	485	505
Solution λ_{max} (nm)	424	424	425	425	425	428
Film λ_{onset} (nm)	500	500	500	500	500	540
Film λ_{max} (nm)	423	415	385	387	385	432
Photoluminescence						
Solution λ_{max} (nm)	504	500	506	514	502	542
Film λ_{max} (nm)	556	560	570	564	560	590
DSC						
Melting temp. (°C)	276	226	237	232	223	218
Crystallization (°C)	206[a]	176	226	216	214	202

[a] Highest crystallization temperature recorded.

The as-cast films were heated for five minutes at 10 °C intervals from 60–200 °C with direct mounting onto a hot plate. No significant change in the absorption profile was observed for compounds **3–6** with linear chains other than a gradual decrease in absorption with temperature increase due to film de-wetting (Fig. S11, ESI†). This suggests that the as-cast films are in a low energy state. Compounds **1** and **2** with branched chains, however, responded more significantly upon thermal annealing. At 60 °C, the appearance of fine structure in the thin film absorption profile of **2** was evident (Fig. S11, ESI†). Compound **1** with 1-ethylpropyl chains responded the most to thermal annealing with the appearance of fine structure accompanied by a blue shift in absorption maximum at 80 °C (Fig. 5A). Using optical microscopy, the thin films were observed at each stage from as-cast up to 200 °C. Nothing was visible up to 100× magnification for compounds **2–6** (Fig. S12, ESI†). Compound **1**, however, displayed large crystalline domains upon thermal annealing at 80 °C which persisted until 120 °C (Fig. 5B), higher annealing temperatures resulted in film de-wetting, likely due to over crystallization. These results imply that the 1-ethylpropryl side chain imparts unique solid-state organization properties on this class of molecule.

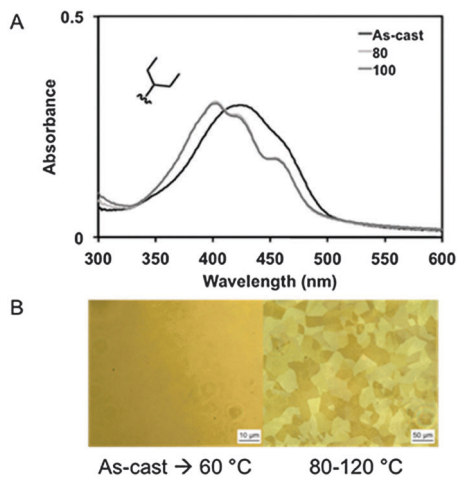

Fig. 5 (A) Absorption profile of as-cast and thermally annealed films of compound **1**. (B) Optical microscopy images of as-cast and annealed films of compound **1** at 100× (left) and 20× (right).

The influence of the alkyl side chain on structure–property relationships was also apparent from drop-cast films of **1–6**, which gave vastly different microscale morphologies (Fig. S15, ESI†). Compounds **1–3** form uneven films composed of large crystals on the order of 10–100 μm. Compounds **4** and **5** form more uniform films composed of smaller crystallites with sizes below 25 μm and 10 μm whereas compound **6** forms amorphous films. These results imply that under slow-drying film formation, the compounds with short 5-carbon chains prefer to aggregate into large crystalline clusters regardless of branching point and symmetry while the utility of longer 6 or 8 carbon atom chains allow for uniform film formation. The bulkier naphthalimide endcap appears to prevent material over crystallization.

Differential scanning calorimetry

To probe the thermal properties of these materials, differential scanning calorimetry (DSC) was implemented (Fig. 6), the data summarized in Table 1. All the melting and crystallization points are in the 200–300 °C range typical of rod-like small π-conjugated molecules.[44] Compound **3** with linear pentyl chains melts at 237 °C. Moving to the branched 1-methylbutyl chain (**2**) results in a slightly decreased melting transition to 226 °C, which is expected due to the branched nature of the chain which is likely disrupting the molecular packing. Compound **1** with the symmetrical branched 1-ethylpropyl chains interestingly displays a dramatically higher melting temperature of 275 °C suggesting that the side chain is promoting strong intermolecular interactions. Increasing chain length from five to six carbons (**4**) results in slight decrease in the melting transition from 237 °C to 232 °C, while going from six to eight (**5**) results in a further decrease in melting temperature to 223 °C consistent with the increase in aliphatic character of the molecule. Upon comparing compound **5** with octylphthalimide endcaps to **6** with octylnaphthalimide terminal units, the melting point decreases further to 218 °C, likely owing to the more twisted solid state structure of **6**, which would in turn weaken the intermolecular π–π interactions.

Interestingly, compound **1** was found to display the largest difference between the melting and crystallization transitions. Upon further investigation of compound **1**, erratic crystallization behaviour was observed (Fig. S16, ESI†). Multiple experiments were run on several samples from different batches and all showed the same melting transition at 276 °C but often several crystallization transitions, below 206 °C (with 206 °C being the highest), were observed. Increasing the cooling time lead to somewhat more consistent results (Fig. S17 and S18, ESI†). This unique behaviour has not been observed in related compounds. Investigation of the half molecule and a fused derivative (*i.e.* naphthalene diimide (NDI)) showed normal behaviour (Fig. S19 and 20, ESI†), thus pointing towards some sort of polymorphism occurring for compound **1**. As a side note, we also attempted to evaluate the thermal behaviour of the well-studied perylene diimide (PDI) derivative but observed no transitions up to 300 °C (the limit of the calorimeter) and could not find any reports in the literature.

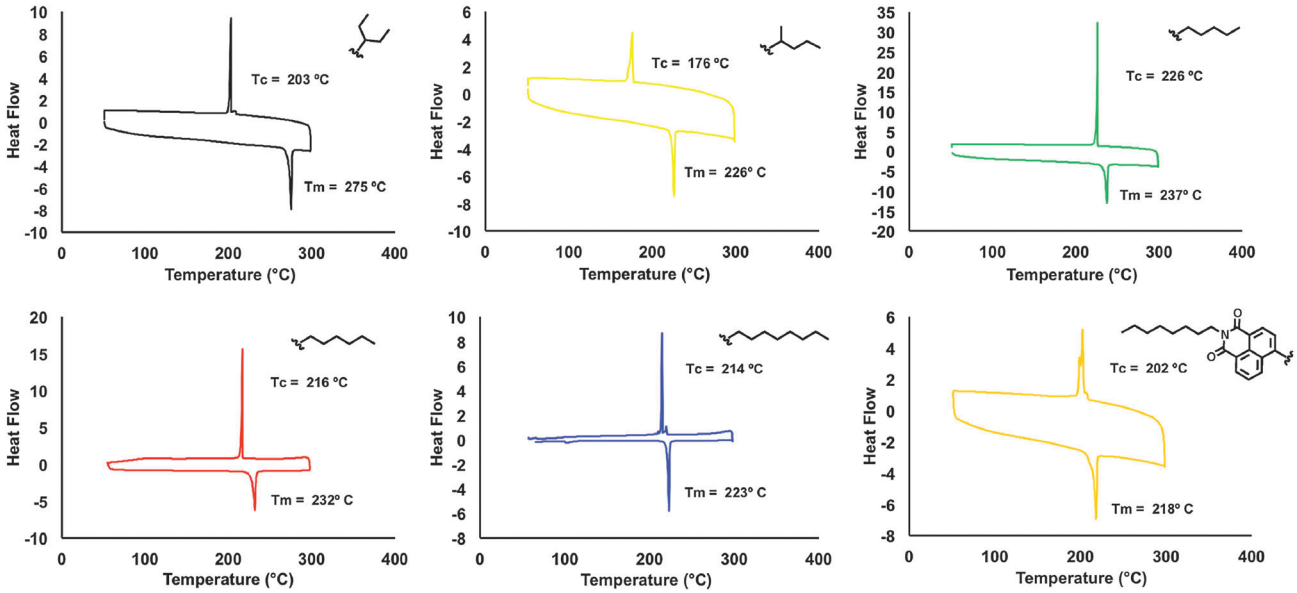

Fig. 6 DSC thermograms of compounds **1–6**.

Considering the importance of this molecule, a more rigorous evaluation of its thermal properties are warranted. Polymorphism has been observed in some related small molecules.[46] These results further illustrate the unique behaviour imparted on the molecule by the 1-ethylpropyl side chains.

Crystal structure determination

With the UV-visible spectroscopic and thermal data in hand indicating dramatic difference in the solid state structure we examined the single crystal structures of each molecule **1–6** and investigated the effect of the various alkyl chains on the resulting packing motifs.

As a general remark, the incorporation of the different alkyl chains (**1–5**) and different end caps (**6**) was found to cause large changes to the way in which the thiophene–phthalimide structure packed in the solid state (Fig. 7). For instance, the longer unbranched alkyl chains found in compounds **4** and **5** seem to promote highly planar configurations of the phthalimide–thiophene backbone in the crystalline form, while the shorter, or branched chains found in compounds **1–3** seem to favour twisting of the bithiophene core with respect to the phthalimide end caps. This ultimately results in the slipped stacked structures for **4** and **5** having the shortest π–π stacking distance by approximately 0.3 Å, but also having the longest slippage along the short molecular axis. For compound **6**, the significant twisting of the end cap with respect to the core is responsible for an elongated π–π stacking distance.

Small molecule **1** bearing 1-ethylpropyl chains crystallized in the monoclinic space group $C2/C$. The bithiophene cores of the molecules of adjacent molecules are parallel within the packing arrangement. The 1-ethylpropyl side chains lie in a perpendicular orientation to the rest of the molecule and presumably because of this they cause the neighbouring phthalimide end-capping units to be twisted with respect to each other to form the zig-zag like arrangement that is necessary in order to minimize interaction between the alkyl chains and maintain a π-stacked structure between the bithiophene cores (Fig. 7, image 1). The angles between the phthalimide end caps and the adjacent thienyl rings are $\sim 13.4^{\circ}$, while the angle between thiophene units within the molecules is 0°. The angle between the planar phthalimide moieties on adjacent molecules is $\sim 25.8^{\circ}$, while the bithiophene cores on adjacent molecules remain parallel with a π–π distance of 3.52 Å.

Small molecule **2** bearing 1-methylbutyl side chains was extremely resistant to crystallization attempts. A crystal suitable for diffraction was obtained by slow evaporation from dichloromethane and the structure was solved in the space group $P2(1)/c$. Despite the high R factor obtained ($R = 0.12$), the structure is still illustrative of the packing arrangement for this system (Fig. 7, image 2). Similar to compound **1**, the branched alkyl chains of compound **2** are oriented perpendicular to the plane of the phthalimide ring and the phthalimide units are twisted with respect to the bithiophene cores at an angle of $\sim 30.6^{\circ}$, while the angle between the thiophene rings in the core of the molecule is 0°. In contrast to **1**, the phthalimide units on adjacent molecules remain parallel between π stacked molecules. The π–π stacking distance between the bithiophene cores on adjacent molecules is 3.74 Å.

Small molecule **3** containing linear C5 alkyl chains crystallized in space group $P\bar{1}$ as needle like crystals. The angle between end-capping phthalimide units and the adjacent thienyl units is $\sim 24.5^{\circ}$ on one side of the molecule and $\sim 16.3^{\circ}$ on the opposite side of the molecule. The angle between thienyl units in the bithiophene core is $\sim 6.1^{\circ}$. The π–π stacking distance between the bithiophene cores of adjacent molecules is 3.52 Å.

The crystal structure of small molecule **4** was previously reported but will be discussed for comparison to the new structures presented in this work.[19] Compound **4** crystallized

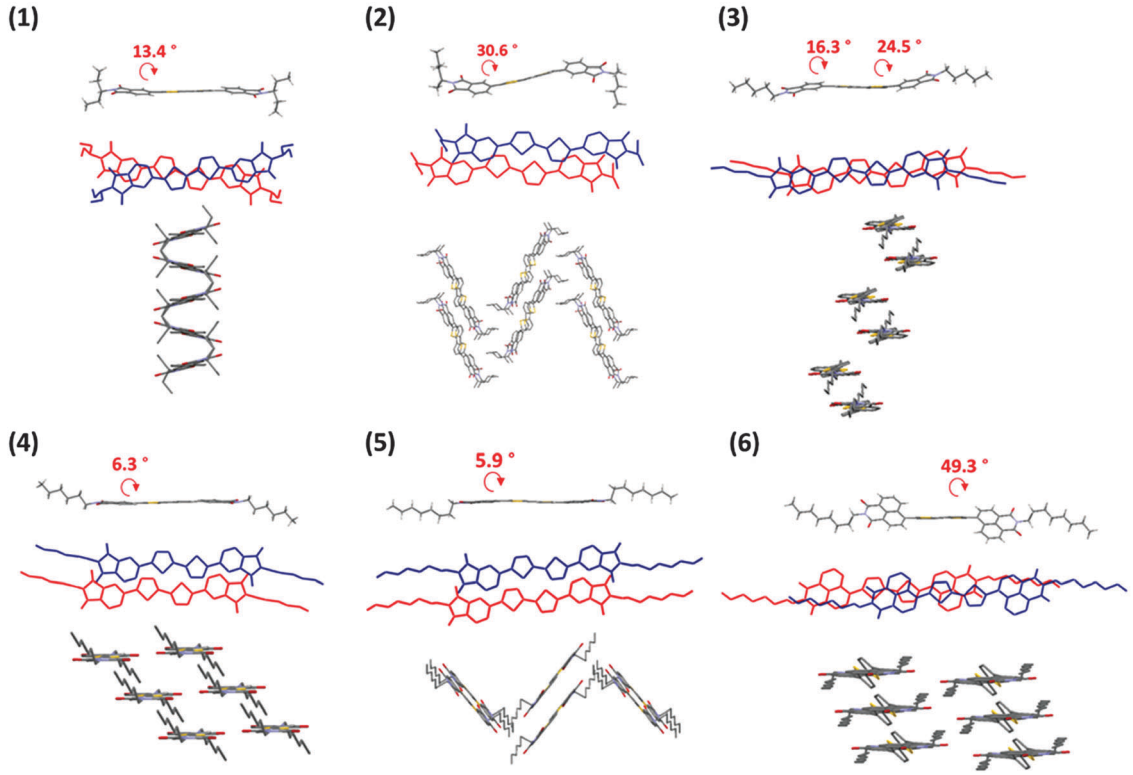

Fig. 7 Single crystal structures of **1–6**. Depiction of a single molecular units of **1–6** from crystal structure data, the dihedral angle between the end-capping phthalimide units and the thienyl linkers is given for each molecule (top). Illustration of the extent of molecular overlap between adjacent molecules within the crystal structures (middle). Packing diagrams illustrating the different packing motifs displayed by **1–6** (bottom).

in space group $P\bar{1}$ as needle-like crystals. A π-stacked packing arrangement was observed with the phthalimide units on adjacent units interacting in a face-to-face fashion (Fig. 7, image 4). The angle between phthalimide end-capping units and the bithiophene core is 6.3°, while the thiophene units in the core of the molecule are co-planar with 0° of twisting between them. The π–π stacking distance between parallel bithiophene cores on adjacent molecules is 3.38 Å; however, there is minimal co-facial interaction between adjacent bithiophene units due to a large slippage along the short molecular axis.

The crystal structure of small molecule **5** was also previously reported by our group.[47] Compound **5** crystallized in space group $P2(1)/n$ as orange needle like crystals and adopted a packing structure resembling that formed by compound **2** (Fig. 7, image 5). The angle between the end-capping phthalimide units and the bithiophene core is ∼5.9°, while the angle between thienyl units in the core of the structure is 0°. The π–π distance between parallel thiophene units on adjacent molecules is 3.25 Å; however, similar to compound **4** which also displays a short π–π stacking distance, there is minimal overlap between adjacent bithiophene units due to relatively large slippage along the short axis of the molecule.

Small molecule **6** crystallized in space group $P\bar{1}$ as large block like crystals. A significant twisting of 49.3° was observed between the naphthalimide terminal groups and the bithiophene core, while the thienyl units in bithiophene core remain co-planar at an angle of 0° (Fig. 7, image 6). Adjacent molecules of **6** within the crystal are aligned such that the bithiophene linkers are parallel with those on an adjacent molecule and lie at a π–π distance of 3.82 Å. While the 1,8-naphthalimide end-capping units on adjacent molecules are twisted with respect to the bithiophene core, they lie parallel to one another on adjacent molecules.

In summary the single crystal data shows a unique packing arrangement for each of the small molecules **1–6**. Small molecules **4** and **5** bearing linear alkyl chains were noted to have the least twisted core structure resulting in ordered face-to-face packing arrangements. Small molecules **4** and **5** were previously shown to be good candidates for electron transporting and hole transporting materials in evaporated thin-film transistor devices, perhaps attributable to their favourable crystal packing.[19] The other structures in this work, containing shorter linear chains (**3**), branched alkyl chains (**1–2**) or a different end-capping unit (**6**) do not assume such planar overall structures, but instead all feature varying degrees of twisting between the end-caps and bithiophene linkers, resulting in larger π–π offsets between adjacent molecules. The 1-ethylpropyl containing compound (**1**) stands out as the only compound of **1–6** where the molecules are aligned in a head-to-tail fashion.

Ellipsometry

The UV-vis absorption profiles of thin films, along with the thermal data and single crystal structures indicated profound differences in the solid state structural ordering of small molecules

1–6. One factor that is known to be important for organic materials is their relative orientation in a thin-film with respect to a given substrate. Thus, it was of interest to probe how these differences in solid-state can affect the organization of these molecules with respect to the substrate onto which they are cast. Grazing incident X-ray diffraction can be used to obtain such information; however, for thin-films the technique is limited to synchrotron radiation, which is not readily available. An alternative technique that gives information regarding the optical anisotropy in organic thin films is variable angle spectroscopic ellipsometry (VASE).[48–50] VASE experiments provide information about the optical anisotropy by measuring the changes in polarized light reflected from a film. A model fitting process is applied in order to extract information about the film including thickness and the optical parameters (refractive index, n and extinction coefficient, k). While ellipsometry may not provide all the same information that a synchrotron X-ray experiment can provide, it has the benefit of being non-destructive (visible wavelengths used for analysis) and in addition the thin film sample need not be crystalline in order to measure the extent of optical anisotropy.

Thin-film samples for VASE analysis were prepared by spin casting hot 10 mg mL^{-1} solutions of **1–6** in $CHCl_3$ onto heated, pre-cleaned ~300 nm SiO_2 layer terminated silicon wafers at 6000 RPM for 30 seconds. Ellipsometry data was collected over the 250–1000 nm range for each of the six films at three different incident angles (55°, 65°, 75°). Two different models were employed to fit the data: (i) B-spline model, which allows arbitrary flexibility in n, k *versus* wavelength and (ii) An anisotropic model, where optical properties can differ in x, y, and z-directions. Within anisotropic model fitting, it is possible to choose either Uniaxial or Biaxial anisotropy. Uniaxial layer describes the anisotropy between in plane (x–y) and out-of-plane (z) directions, while a biaxial anisotropy allows variation in all directions. Representative fits of the model to the data are provided in the ESI.† Initially, the data was fitted with B-spline model and a reasonably good fit was found. The B-spline model was then converted to a uniaxial anisotropic model where optical properties in each direction was seeded with the parameters from the B-spline model. Utilization of this model for the fitting process further improved the fitting and additionally yielded the anisotropic information. The quality of fitting was judged by the mean square error (MSE) values. The film anisotropy was confirmed by taking multiple measurements at different locations (5) per sample and rotating the sample between measurements by 90°.

Both the simple Uniaxial and Biaxial fitting option resulted in comparable results in terms of film thickness, and optical parameters as well as the MSE (see ESI† for a representative fit). However, Biaxial fitting gave additional information about the X–Y plane anisotropy. All samples except for small molecule **1** exhibited no X–Y plane anisotropy, which is not uncommon for spin-cast organic films.[49] That is, the samples were found to be isotropic in the in-plane direction (X–Y) but all samples exhibited anisotropy with significant differences in the optical properties between the in-plane and the out-of-plane directions. The absence of in plane (xy) anisotropy is further confirmed by taking multiple measurements (5) per sample rotating the sample by 90° in the xy plane prior to each measurement and resulted in no difference to the fitted data. Therefore, Uniaxial anisotropic fitting results have been summarized and presented through this paper for simplification.

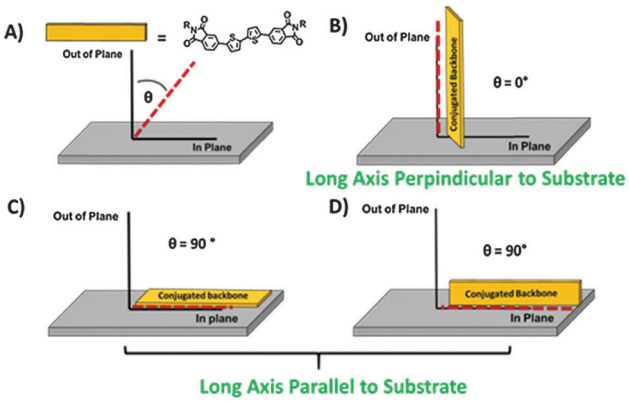

Fig. 8 Using the extracted optical constants from ellipsometry data, it is possible to determine the relative orientation (parallel or perpendicular) of the long axis of the conjugated molecule (assuming the transition dipole lies along this axis).

The VASE data highlights the differences in optical anisotropy for the thin films made from **1–6**. Firstly, the differences in the calculated extinction coefficients k_{in} *vs.* k_{out} (Fig. 8B) in the in-plane and out of plane directions were used to calculate an orientation parameter (S), following the procedure in the work by Schünemann *et al.*[48] In general when $k_{out} \neq k_{in}$ the sample is said to have optical anisotropy (Fig. 9).

Assuming that the transition dipole moment lies along the long axis of the molecule,[48] an S value of ~1 indicates that the

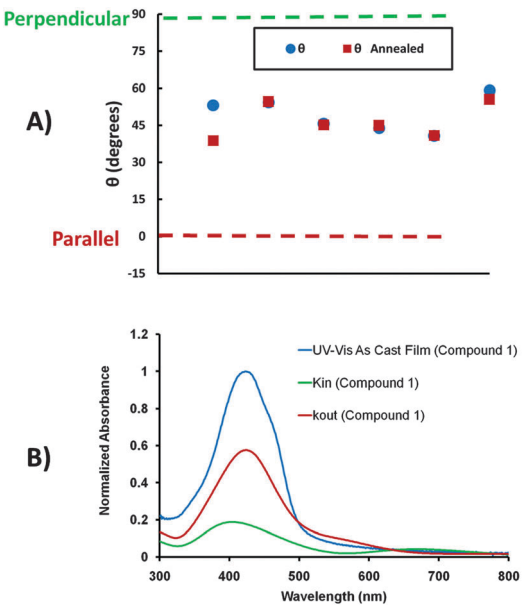

Fig. 9 (A) Plot of the orientation angles (θ) found for each film (B) comparison of pseudo optical coefficients with experimental UV-Vis data. The differences in optical constant values in the in-plane and out of plane directions were used to describe the optical anisotropy in the thin films.

Table 2 Ellipsometry data

	As cast films					Annealed films				
Compound	Thickness (nm)	MSE	K_{out}/K_{in}	S	θ	Thickness (nm)	MSE	K_{out}/K_{in}	S	θ
1	33	8.82	1.17	0.039	53	39	6.6	3.10	0.412	39
2	33	7.37	1.03	0.010	54	31	9.2	1.15	0.003	55
3	26	6.40	2.71	0.360	41	31	5.7	2.68	0.359	41
4	27	5.70	2.15	0.277	44	27	6.1	2.01	0.251	45
5	31	6.40	1.83	0.230	46	31	6.3	1.99	0.247	45
6	33	6.11	0.72	−0.104	59	33	5.8	0.95	−0.019	56

molecules have their long axis aligned perpendicular to the substrate. An S value of ~ -0.5 indicates that the molecules have their long axis lying parallel to the substrate and an S value of 0 indicates no preferred orientation. In general, small molecules **3–6** have orientation parameters that deviate further from 0 than those of the branched chain compounds **1–2** in the as cast films. That is, **3–6** were found to be isotropic in the in-plane direction but exhibited anisotropy with significant differences in the properties between the in-plane and out-of-plane directions (Table 2).

The S value can also be related to the orientation angle (θ) which describes the average relative orientation of the molecules with respect to the substrate (Fig. 8).[48] The tabulated S and θ values and orientation angles can be found in Table 2 along with the film thicknesses and MSE values from the ellipsometry model fitting. In general, the orientation angle indicated that each of the molecules **1–6** have, on average, a tilted orientation with respect to the substrate for both the as-cast and the annealed films. The average orientation of the small molecules was found to be tilted between 41° and 59° from the substrate normal, and for all molecules except for **1**, minimal changes to the ratio of the extracted out of plane and in plane extinction coefficients upon annealing were observed.

UV-visible spectroscopy and optical microscopy showed that compound **1** undergoes considerable changes to its solid state structure upon annealing (Fig. 4 and 5). These observations correlate well with the VASE data where compound **1** was found to have increased optical anisotropy in the thin film after annealing, suggesting a more ordered structure.

Organic electronic devices

In an effort to correlate materials properties to electrical performance, compounds **1–6** were used as the semiconducting material in field effect transistors (FETs). As previously noted, evaporated films of compound **4** and **5** were found to be highly crystalline, adopt a similar packing arrangement to the single crystal structure, and when used as the active component in bottom-gate, top-contact (BGTC) FETs, good device performance was observed. In this present study we focused our attention on solution processed thin-films for which forming uniform films with proper alignment of the semiconductor can be challenging. Several attempts were made at forming working devices. Using a bottom gate, bottom contact configuration with Si/SiO_2 modified with dodecyltrichlorosilane (DDTS) we were unable to form uniform thin-films and thus transistor performance was unreliable. Fig. S23 (ESI†) shows the devices with uneven surface coverage. Switching to pre-patterned interdigitated ITO substrates we were able to successfully form uniform thin-films, but unfortunately these films did not hold up to the deposition of a poly(methyl methacrylate) (PMMA) gate dielectric. Thus we resorted to using a BGTC architecture with no surface treatments of the silicon oxide substrates. With this configuration we were able to improve the surface wetting and form uniform films of compounds **1–6** from $CHCl_3$ solutions. In addition these films most closely mimic those used for the UV-vis spectroscopy and VASE experiments. Full details can be found in the ESI.† No FET behaviour was observed for as-cast films. Upon thermal annealing only films of compound **6** turned on. N-type FET behaviour was observed with the characteristics: linear mobility μ_{lin} ($cm^2\ V^{-1}\ s^{-1}$) = $3.3 \times 10^{-4} \pm 1.0 \times 10^{-4}$, V_T = 70 ± 2 V and $I_{on/off}$ = 50 ± 20 (Fig. S24, ESI†). The lack of FET behaviour is not surprising for these solution processed thin-films as the VASE experiments indicated that none of the films adopted a preferred parallel or perpendicular orientation with respect to the substrate. Therefore due to the molecular nature of the compounds and directionality in their crystal structures, the solution processed thin-film morphology and relative orientation of the crystal grains relative to the source-drain electrode are likely imperative to device performance. In addition bare Si/SiO_2 was used for which electron traps from hydroxyl groups in the form of silanols can hinder electron transport. Further investigations into the spin casting conditions, surface treatments and annealing method need be undertaken to investigate the relationship between the charge transport characteristics of this class of compounds and their thin-film morphology.

Conclusions

We have presented on the optimized synthesis and characterization of a family of aryl imide based organic small molecules and investigated structure–property–function relationships. The small molecules were constructed with a bithiophene core and phthalimide or naphthalimide end-capping units. This type of architecture has previously been demonstrated as a useful electron transport material in organic field-effect transistor and organic solar cells. These molecules proved to be very straight forward to synthesize and purify. In particular a new synthesis has been reported where installation of alkyl groups *via* a condensation reaction is the final step. This can allow for the rapid synthesis of a library of compounds with minimal purification required.

Through the variation of the solubilizing alkyl chain length and branching point, molecular properties were easily tuned. While all compounds had similar onsets of optical absorption, varying the alkyl chain or end capping unit influenced the absorption maxima. Compounds **3–5** with phthalimide end-caps functionalized with linear side chains exhibited large hypsochromic shifts in absorption maxima when transitioning from solution to film, where functionalization with branched side chains (**1–2**) or bulkier naphthalimide end caps (**6**) resulted in slight bathochromic shifts. Thermal annealing had minimal effect on the optical profile of compounds **3–5** but those of **1**, **2**, and **6** all blue shifted significantly indicating a change in molecular orientation. Thus greater control of self-assembly tendencies is realized with increased steric bulk about the π-conjugated backbone. In particular compound **1** exhibited the largest changes in both peak maxima and absorption profile. This was attributed to crystallization of film as seem through the emergence of large well-defined domains *via* optical microscopy. Curiously, compounds **2–6** were only observed as amorphous films.

The melting and crystallization behaviour of compounds **2–6** followed an obvious trend where a decrease in aliphatic character and end-cap size lead to an increase in thermal transition temperatures, owing to a greater ratio of intermolecular π–π interactions likely occurring in the solid-state. Interestingly, small molecule **1** bearing 1-ethylpropyl side chains had the highest melting transition which could point towards some sort of unique interdigitating of the ethyl chains. Compound **1** also exhibited erratic crystallization behaviour despite consistent melting behaviour over several trials with differing heating rates. This unexplained observation requires further investigation.

Single crystal X-ray diffraction showed that compounds with longer linear alkyl chains (**4–5**) tend to take on less distorted backbone configurations than those with shorter (**3**), branched (**1–2**) or a bulkier end-capping unit (**6**). This leads to **4** and **5** having strong face-to-face stacking interactions and the others offset stacking interactions.

Variable angle spectroscopic ellipsometry experiments illustrated the extent of optical anisotropy in the thin films of **1–6** on silicon substrates, where the studied systems were shown to exhibit uniaxial anisotropy. Following thermal annealing, compound **1** displayed a tendency to adopt a slightly more perpendicular orientation with respect to the substrate compared to the as-cast film whereas all other films remained largely unchanged.

Unfortunately we could not draw correlations of materials properties to electronic performance using organic field effect transistors with solution processed active layers. All compounds did not wet surface treated silicon oxide substrates and transistors fabricated without surface treatments showed little or no FET behaviour. Thus we can conclude that this series of molecules is better suited for evaporated devices or high molecular weight (*e.g.* polymers or long oligomers) should be considered as processing agents.

In summary, the aryl imide-thiophene architecture is highly responsive to changes in the solubilizing alkyl chains. In each experiment the 1-ethylpropyl side chain imparts unique self-assembly properties that are not trivial to understand and presents itself as an interesting unit to study.

Experimental

Full experimental details including materials and methods, instrumentation, and NMR spectra can be found in the ESI.†

Synthesis of 2,2′-bithiophene

Prepared according to literature procedure.[51]

Synthesis of 4-bromo-1-ethylpropylphthalimide (EP-Phth)

A 20 mL microwave vial was loaded with 4-bromophthalic anhydride (500 mg, 2.2 mmol) and 1-ethylpropylamine (231 mg, 2.6 mmol) in acetic acid (10 mL). The reaction vial was sealed and heated under microwave irradiation for five minutes at 120 °C followed by 15 minutes at 180 °C. The cooled reaction mixture was then poured into H_2O (100 mL) and stirred for 3 hours. The white precipitate was isolated by vacuum filtration, washed with 3 : 1 water : methanol and dried *in vacuo* to yield a white solid (585 mg, 1.98 mmol, 90% yield). ^{1}H NMR: spectroscopic data is in accordance with those previously reported in the literature.[22]

Synthesis of 1

A 20 mL microwave vial was loaded with **EP-Phth** (1.065 g, 3.6 mmol), 2,2′-bithiophene (0.300 g, 1.80 mmol), potassium carbonate (0.622 g, 4.50 mmol), pivalic acid (0.056 g, 0.55 mmol), and SiliaCat® DPP-Pd catalyst (360 mg, 0.09 mmol). Benchtop DMA (12 mL) was added and to mixture and the reaction vessel was sealed and heated in an oil bath at 80 °C for 24 hours. The cooled reaction mixture was then poured into H_2O (150 mL) and stirred overnight. The orange precipitate was collected *via* suction filtration, dissolved in ethyl acetate and filtered through a silica plug to remove the heterogeneous catalyst. Any remaining material in the silica was pulled through with 50 : 50 ethyl acetate : dichloromethane. Solvent was removed under reduced pressure to yield an orange solid, which was collected *via* suction filtration washing with methanol. The crude material was purified by recrystallization from THF (1 mL/50 mg) yielding a bright orange solid (843 mg, 1.41 mmol, 78% yield). ^{1}H NMR: spectroscopic data is in accordance with those previously reported in the literature.[22]

Synthesis of 4-bromo-1-methylbutylphthalimide (MB-Phth)

The same reaction conditions as reported for **1EP-Phth** were utilized, substituting ethylpropyl amine for 2-amino-pentane. The product was isolated as a white solid (85% yield). ^{1}H NMR ($CDCl_3$): δ7.96 (m ov, 1H), 7.77 (m ov, 2H), 4.36 (m, 1H), 2.05 (m, 1H), 1.71 (m, 1H), 1.47 (d, $^1J_{H-H}$ = 6.9 Hz, 3H), 1.28 (m, 2H), 0.91 (t, 3H) ^{13}C NMR ($CDCl_3$): δ167.7, 167.1, 136.7, 133.7, 130.5, 128.6, 126.4, 124.4, 47.5, 35.7, 19.9, 18.6, 13.6 theoretical: 14 peaks, experimental: 13 peaks MS (APCI-TOF): *m*/*z* 296.2. calcd 296.0.

Synthesis of 2

The same reaction conditions, work up, and purification as reported for **1** were utilized, substituting **1EP-Phth** for **MB-Phth**.

The product was isolated as an orange solid (76% yield). ^{1}H NMR ($CDCl_3$): δ8.04 (m, 1H), 7.91 (m ov, 1H), 7.84 (m ov, 1H), 7.45 (d, $^1J_{H-H}$ = 3.9 Hz, 1H), 7.29 (d, $^1J_{H-H}$ = 3.9 Hz, 1H), 4.41 (m, 1H), 2.10 (m, 1H), 1.74 (m, 1H), 1.50 (d, $^1J_{H-H}$ = 7.0 Hz, 3H), 1.31 (m, 2H), 0.94 (t, 3H) ^{13}C NMR ($CDCl_3$): δ 168.2, 168.1, 141.4, 139.5, 138.3, 133.2, 130.2, 126.2, 125.6, 123.8, 119.6, 47.4, 35.8, 20.0, 18.7, 13.7 theoretical: 17 peaks, experimental: 16 peaks MS (APCI-TOF): *m*/*z* 596.8. calcd 597.2.

Synthesis of 4-bromo-2-pentylphthalimide (P-Phth)

The same reaction conditions as reported for **1EP-Phth** were utilized, substituting ethylpropyl amine for 1-aminopentane. The product was isolated in quantitative yield as a white solid. ^{1}H NMR ($CDCl_3$): δ 7.99 (m ov, 1H), 7.79 (m ov, 2H), 3.68 (t, 2H), 1.68 (m, 2H), 1.35 (m, 4H) 0.91 (t, 3H) ^{13}C NMR ($CDCl_3$): δ 167.6, 167.0, 136.8, 133.8, 130.7, 128.7, 126.5, 124.5, 38.3, 28.9, 28.2, 22.2, 13.9 theoretical: 14 peaks, experimental: 13 peaks MS (APCI-TOF): *m*/*z* 296.2. calcd 296.0.

Synthesis of 3

The same reaction conditions, work up, and purification as reported for **1** were utilized, substituting **1EP-Phth** for P-Phth. The product was isolated in as an orange solid (75% yield). ^{1}H NMR ($CDCl_3$):δ8.10 (m, 1H), 7.89 (m ov, 2H), 7.46 (d, $^1J_{H-H}$ = 3.9 Hz, 1H) 7.29 (d, $^1J_{H-H}$ = 3.9 Hz, 1H), 3.71 (t, 2H), 1.43 (q, 2H), 1.37 (m, 4H) 0.92 (t, 3H) ^{13}C NMR ($CDCl_3$): δ 168.1, 168.0, 141.4, 139.6, 138.3, 133.4, 130.4, 130.2, 126.3, 125.6, 123.9, 119.7, 38.2, 29.0, 28.3, 22.3, 13.9 theoretical: 17 peaks, experimental: 17 peaks MS (APCI-TOF): *m*/*z* 596.76. calcd 597.2.

Synthesis of 4 and 5

Prepared according to literature procedure.[17,19]

Synthesis of 5,5′-bis(trimethylstannyl)-2,2′-bithiophene

Prepared according to literature procedure.[52]

Synthesis of 6,6′-([2,2′-bithiophene]-5,5′-diyl)bis(naphthalimide) (Nap-Th$_2$-Nap)

4-Bromo-1,8-naphthalic anhydride (193 mg, 0.70 mmol), 5,5′-bis(trimethylstannyl)-2,2′-bithiophene (186 mg, 0.38 mmol), and $Pd(PPh_3)_4$ (47 mg, 4 mol%) were added to a 20 mL microwave vial with anhydrous toluene (15 mL). The vial was sealed under N_2 and placed in a microwave reactor for five minutes at 100 °C followed by 20 minutes at 170 °C. The cooled reaction mixture was poured into methanol (100 mL) stirred for one hour. The resulting fine brown powder was collected *via* vacuum filtration and heated up in isopropanol (100 mL). The material was then recollected and heated up in THF (100 mL) and collected as a dark red-brown solid (172 mg, 0.31 mmol, 81% yield). ^{1}H NMR/^{13}C NMR: NMR data was not obtained due to low solubility MS (APCI-TOF): *m*/*z* 558.6. calcd 559.0.

Synthesis of 6

Nap-Th$_2$-Nap (107 mg, 0.19 mmol), anhydrous dimethylformamide (3 mL) and an excess of octylamine (391 mg, 3.0 mmol) were added to a 10 mL microwave vial. The reaction mixture was sealed under N_2 and placed in a microwave reactor for 20 minutes at 180 °C. The cooled reaction mixture was poured into H_2O and stirred for two hours. The resulting green material was filtered then dissolved up in dichloromethane and sent through a short silica plug. The solvent was removed under reduced pressure and the resultant orange flakes were slurried in 3 : 1 H_2O : methanol and isolated using vacuum filtration (129 mg, 0.17 mmol, 89% yield). ^{1}H NMR ($CDCl_3$): δ 8.75 (d, $^1J_{H-H}$ = 5.1 Hz, 1H), 8.71 (d, $^1J_{H-H}$ = 4.3 Hz, 1H), 8.67 (d, $^1J_{H-H}$ = 4.5 Hz, 1H), 7.91 (d, $^1J_{H-H}$ = 4.6 Hz, 1H), 7.84 (t, 1H), 7.45(d, $^1J_{H-H}$ = 2.2 Hz, 1H), 7.37 (d, $^1J_{H-H}$ = 2.2 Hz, 1H), 4.24 (t, 2H), 1.79 (m, 2H), 1.51–1.32 (m, 10H) 0.92 (t, 3H) ^{13}C NMR ($CDCl_3$): δ 164.3, 164.1, 139.6, 139.1, 138.5, 132.2, 131.7, 130.9, 130.1, 129.2, 128.6, 127.6, 125.2, 123.4, 122.5, 40.8, 32.1, 29.6, 29.5, 28.4, 27.4, 22.9, 14.3 theoretical: 24 peaks, experimental: 23 peaks MS (APCI-TOF): *m*/*z* 781.0. calcd 781.0.

Synthesis of 5,5′-([2,2′-bithiophene]-5,5′-diyl)bis(phthalimide) (Phth-Th$_2$-Phth)

The same reaction conditions as reported for **Nap-Th$_2$-Nap** were utilized, substituting 4-bromo-1,8-naphthalic anhydride for 4-bromophthalic anhydride. The product was isolated as a fine brown powder (56% yield). ^{1}H NMR/^{13}C NMR: NMR data was not obtained due to low solubility MS (APCI-TOF): *m*/*z* 458.5. calcd 459.0.

Alternative synthesis of 5

The same reaction conditions as reported for **6** were utilized, substituting **Nap-Th$_2$-Nap** for **Phth-Th$_2$-Phth**. The product was isolated as an orange solid (47% yield). ^{1}H NMR: spectroscopic data is in accordance with those previously reported in the literature.[17,19]

Acknowledgements

GCW acknowledges the Canada Research Chairs Program and the Natural Science and Engineering Council of Canada (NSERC RGPIN 435715-2013) for financial support. ADH is grateful for an NSERC scholarship. AJP is grateful for a QEII scholarship. Bin Sun and Yuning Li (University of Waterloo) are acknowledge for fabrication and testing of BGBC OFET devices. Maxwell Reinhardt (Ossila Ltd) is acknowledged for fabrication of BGTC ITO OFETs devices and BGTC Si/SiO_2 devices.

Notes and references

1 S. R. Forrest, *Nature*, 2004, **428**(6986), 911.
2 M. Berggren, D. Nilsson and N. D. Robinson, *Nat. Mater.*, 2007, **6**(1), 3.
3 B. Kippelen and J.-L. Brédas, *Energy Environ. Sci.*, 2009, **2**(3), 251.
4 Y.-J. Cheng, S.-H. Yang and C.-S. Hsu, *Chem. Rev.*, 2009, **109**(11), 5868.
5 A. Facchetti, *Chem. Mater.*, 2011, **23**(3), 733.
6 Y. Fang, A. K. Pandey, A. M. Nardes, N. Kopidakis, P. L. Burn and P. Meredith, *Adv. Energy Mater.*, 2013, **3**(1), 54.

7 J. Mei and Z. Bao, *Chem. Mater.*, 2014, **26**(1), 604.
8 T. Lei, J.-Y. Wang and J. Pei, *Chem. Mater.*, 2014, **26**(1), 594.
9 A. Babel and S. A. Jenekhe, *Synth. Met.*, 2005, **148**(2), 169.
10 H. Bronstein, D. S. Leem, R. Hamilton, P. Woebkenberg, S. King, W. Zhang, R. S. Ashraf, M. Heeney, T. D. Anthopoulos, J. de Mello and I. McCulloch, *Macromolecules*, 2011, **44**(17), 6649.
11 L. Ding, H.-B. Li, T. Lei, H.-Z. Ying, R.-B. Wang, Y. Zhou, Z.-M. Su and J. Pei, *Chem. Mater.*, 2012, **24**(10), 1944.
12 H. Ebata, T. Izawa, E. Miyazaki, K. Takimiya, M. Ikeda, H. Kuwabara and T. Yui, *J. Am. Chem. Soc.*, 2007, **129**(51), 15732.
13 C. Cabanetos, A. El Labban, J. A. Bartelt, J. D. Douglas, W. R. Mateker, J. M. J. Fréchet, M. D. McGehee and P. M. Beaujuge, *J. Am. Chem. Soc.*, 2013, **135**(12), 4656.
14 A. T. Yiu, P. M. Beaujuge, O. P. Lee, C. H. Woo, M. F. Toney and J. M. J. Fréchet, *J. Am. Chem. Soc.*, 2012, **134**(4), 2180.
15 C. Piliego, T. W. Holcombe, J. D. Douglas, C. H. Woo, P. M. Beaujuge and J. M. J. Fréchet, *J. Am. Chem. Soc.*, 2010, **132**(22), 7595.
16 S. Wood, J.-H. Kim, D.-H. Hwang and J.-S. Kim, *Chem. Mater.*, 2015, **27**(12), 4196.
17 A. D. Hendsbee, C. M. Macaulay and G. C. Welch, *Dyes Pigm.*, 2014, **102**, 204.
18 A. F. Eftaiha, J.-P. Sun, A. D. Hendsbee, C. Macaulay, I. G. Hill and G. C. Welch, *Can. J. Chem.*, 2014, **92**, 932.
19 J.-P. Sun, A. D. Hendsbee, A. F. Eftaiha, C. Macaulay, L. R. Rutledge, G. C. Welch and I. G. Hill, *J. Mater. Chem. C*, 2014, **2**(14), 2612.
20 A. D. Hendsbee, J.-P. Sun, T. M. McCormick, I. G. Hill and G. C. Welch, *Org. Electron.*, 2015, **18**, 118.
21 S. M. McAfee, J. S. J. McCahill, C. M. Macaulay, A. D. Hendsbee and G. C. Welch, *RSC Adv.*, 2015, **5**(33), 26097.
22 A. D. Hendsbee, S. M. McAfee, J.-P. Sun, T. M. McCormick, I. G. Hill and G. C. Welch, *J. Mater. Chem. C*, 2015, **3**(34), 8904.
23 O. K. Kwon, J.-H. Park, D. W. Kim, S. K. Park and S. Y. Park, *Adv. Mater.*, 2015, **27**, 1951.
24 O. K. Kwon, J.-H. Park, S. K. Park and S. Y. Park, *Adv. Energy Mater.*, 2015, **5**(1), 1400929.
25 J. T. Bloking, T. Giovenzana, A. T. Higgs, A. J. Ponec, E. T. Hoke, K. Vandewal, S. Ko, Z. Bao, A. Sellinger and M. D. McGehee, *Adv. Energy Mater.*, 2014, **4**(12), 1301426.
26 J. T. Bloking, X. Han, A. T. Higgs, J. P. Kastrop, L. Pandey, J. E. Norton, C. Risko, C. E. Chen, J.-L. Brédas, M. D. McGehee and A. Sellinger, *Chem. Mater.*, 2011, **23**(24), 5484.
27 A. D. Hendsbee, J.-P. Sun, L. R. Rutledge, I. G. Hill and G. C. Welch, *J. Mater. Chem. A*, 2014, **2**(12), 4198.
28 X. Guo, F. S. Kim, S. A. Jenekhe and M. D. Watson, *J. Am. Chem. Soc.*, 2009, **131**(21), 7206.
29 S. M. McAfee, J. M. Topple, A.-J. Payne, J.-P. Sun, I. G. Hill and G. C. Welch, *ChemPhysChem*, 2015, **16**, 1190.
30 S. M. McAfee, J. M. Topple, J.-P. Sun, I. G. Hill and G. C. Welch, *RSC Adv.*, 2015, **5**(97), 80098.
31 X. Zhang, J. Zhang, H. Lu, J. Wu, G. Li, C. Li, S. Li and Z. Bo, *J. Mater. Chem. C*, 2015, **3**(27), 6979.
32 J. Zhang, G. Li, C. Kang, H. Lu, X. Zhao, C. Li, W. Li and Z. Bo, *Dyes Pigm.*, 2015, **115**, 181.
33 D. Gudeika, A. Michaleviciute, J. V. Grazulevicius, R. Lygaitis, S. Grigalevicius, V. Jankauskas, A. Miasojedovas, S. Jursenas and G. Sini, *J. Phys. Chem. C*, 2012, **116**(28), 14811.
34 T. B. Singh, S. Erten, S. Günes, C. Zafer, G. Turkmen, B. Kuban, Y. Teoman, N. S. Sariciftci and S. Icli, *Org. Electron.*, 2006, **7**(6), 480.
35 S. R. Puniredd, A. Kiersnowski, G. Battagliarin, W. Zajączkowski, W. W. H. Wong, N. Kirby, K. Müllen and W. Pisula, *J. Mater. Chem. C*, 2013, **1**(13), 2433.
36 A. Sharenko, C. M. Proctor, T. S. van der Poll, Z. B. Henson, T.-Q. Nguyen and G. C. Bazan, *Adv. Mater.*, 2013, **25**(32), 4403.
37 A. Sharenko, D. Gehrig, F. Laquai and T.-Q. Nguyen, *Chem. Mater.*, 2014, **26**(14), 4109.
38 R. Singh, E. Aluicio-Sarduy, Z. Kan, T. Ye, R. C. I. MacKenzie and P. E. Keivanidis, *J. Mater. Chem. A*, 2014, **2**(35), 14348.
39 T. K. An, S.-H. Hahn, S. Nam, H. Cha, Y. Rho, D. S. Chung, M. Ree, M. S. Kang, S.-K. Kwon, Y.-H. Kim and C. E. Park, *Dyes Pigm.*, 2013, **96**(3), 756.
40 S. Kim, T. K. An, J. Chen, I. Kang, S. H. Kang, D. S. Chung, C. E. Park, Y.-H. Kim and S.-K. Kwon, *Adv. Funct. Mater.*, 2011, **21**(9), 1616.
41 W. J. Harrison, D. L. Mateer and G. J. T. Tiddy, *J. Phys. Chem.*, 1996, **100**(6), 2310.
42 R. Capelli, F. Dinelli, S. Toffanin, F. Todescato, M. Murgia, M. Muccini, A. Facchetti and T. J. Marks, *J. Phys. Chem. C*, 2008, **112**(33), 12993.
43 X. Li, B. K. C. Kjellander, J. E. Anthony, C. W. M. Bastiaansen, D. J. Broer and G. H. Gelinck, *Adv. Funct. Mater.*, 2009, **19**(22), 3610.
44 M. Durso, D. Gentili, C. Bettini, A. Zanelli, M. Cavallini, F. D. Angelis, M. G. Lobello, V. Biondo, M. Muccini, R. Capelli and M. Melucci, *Chem. Commun.*, 2013, **49**(39), 4298.
45 Y. M. Sun, Y. Q. Ma, Y. Q. Liu, Y. Y. Lin, Z. Y. Wang, Y. Wang, C. A. Di, K. Xiao, X. M. Chen, W. F. Qiu, B. Zhang, G. Yu, W. P. Hu and D. B. Zhu, *Adv. Funct. Mater.*, 2006, **16**(3), 426.
46 L. Maini, F. Gallino, M. Zambianchi, M. Durso, M. Gazzano, K. Rubini, D. Gentili, I. Manet, M. Muccini, S. Toffanin, M. Cavallini and M. Melucci, *Chem. Commun.*, 2015, **51**(11), 2033.
47 A. D. Hendsbee, C. M. Macaulay and G. C. Welch, *Dyes Pigm.*, 2014, **102**(0), 204.
48 C. Schünemann, D. Wynands, K.-J. Eichhorn, M. Stamm, K. Leo and M. Riede, *J. Phys. Chem. C*, 2013, **117**(22), 11600.
49 M. Campoy-Quiles, P. G. Etchegoin and D. D. C. Bradley, *Phys. Rev. B: Condens. Matter Mater. Phys.*, 2005, **72**(4), 045209.
50 D. Wynands, M. Erber, R. Rentenberger, M. Levichkova, K. Walzer, K.-J. Eichhorn and M. Stamm, *Org. Electron.*, 2012, **13**(5), 885.
51 C.-Y. Kuo, Y.-C. Huang, C.-Y. Hsiow, Y.-W. Yang, C.-I. Huang, S.-P. Rwei, H.-L. Wang and L. Wang, *Macromolecules*, 2013, **46**(15), 5985.
52 C.-H. Cho, H. Kang, T. E. Kang, H.-H. Cho, S. C. Yoon, M.-K. Jeon and B. J. Kim, *Chem. Commun.*, 2011, **47**(12), 3577.